



Effect of External Magnetic Field on the Surface Morphology of SnO₂ nanomaterial

Jonathan Briones^{1*}, Gwen Castillon¹, Michael Delmo¹, and Gil Nonato Santos¹,

¹Physics Department, De La Salle University

* Corresponding Author: jonathan_briones@dlsu.edu.ph

Abstract: The study examined the effect of external magnetic field (EMF) on the surface morphology and elemental composition of tin oxide (SnO₂) nanomaterials using Scanning Electron Microscopy (SEM) and Energy Dispersive X-ray (EDX) Analysis. The study also explored the CO₂ gas sensing capability of the synthesized nanomaterials. The nanomaterials were produced using the HVPG deposition method where fused quartz tubes containing 35 mg of SnO₂ powder were evacuated down to 10⁻⁶ Torr and annealed at a temperature of 1,200 °C at growth time of 8 hours, and ramp time of 40 minutes using a Thermolyne horizontal tube furnace. The magnetic field intensity was varied as well as the position of the permanent magnet along the tube. Wire-like structures dubbed as “nanoferns” with great surface to volume ratio together with agglomerated nanoparticles were seen on the section of the tube applied with EMF of 3100 gauss. Lower density but higher diameter of wire-like structures were found when the same EMF intensity was supplied to a section with a higher temperature, nearer to the furnace. On the other hand, lower magnetic field intensity (1900 gauss) was observed to produce smaller density and length of structures. Application of EMF helps control the morphology of nanostructures however the thermal gradient influences the material more significantly than the EMF. EDX confirms the presence of tin oxide on the structures formed in sections of the tube. The nanostructures synthesized with applied EMF under the optimized condition were found to be sensitive to CO₂ gas exposure.

Key Words: magnetic field; tin oxide; nanomaterial; CO₂ gas sensor; HVPG deposition technique

1. INTRODUCTION

Nanotechnology is the engineering of functional systems at the molecular scale. It is becoming a big field in science with numerous applications for home, electronics industry, health and medicine among others, owing to enhanced properties of materials being lighter, stronger, smarter, cheaper, cleaner, and long lasting (De Mesa et al, 2012). Among these technologies, devices has been developed in gas sensing.

There are many gas sensor available, however new researches are conducted on

nanomaterial based sensors because of its enhanced sensitivity and low cost characteristics. Among the materials used for these gas sensing applications are metal oxides due to their availability and practicality as compared to noble gas or rare earth materials counterpart. One of the popular metal oxides is SnO₂.

SnO₂, an n-type wide band gap semiconductor with rutile crystal structure, is a key functional material known for a variety of applications (optoelectronic devices, anode material for lithium-based batteries and liquid crystal displays) one of which is gas sensing (Delos Reyes et al, 2011; Batzill and Diebold, 2005; Das and Jayaraman, 2014). Gas sensing capabilities of SnO₂

nanostructures has been widely studied due to their sensitive conductivity changes upon gas reaction and adsorption. Its importance spans many aspects such as personal safety and security, detection and diagnosis of pollutants and poisons, health, semiconductor processing, agriculture, and automotive and aerospace industries (Bancolo, 2011; Kolmakov and Moskovits, 2004; Cadena et al, 2007). Gas detection is found to be more sensitive if the material used is made of 1D nanomaterials (i.e. nanowires with diameter below 100nm). This is because of its high surface to volume ratio (Kolmakov and Moskovits, 2004; Ji et al, 2010)

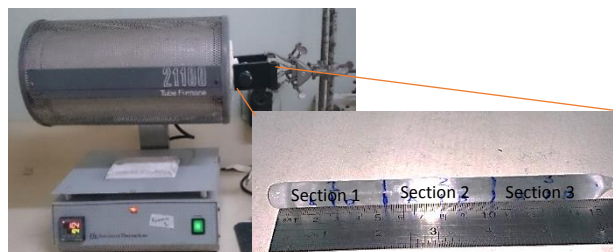
Different morphologies of SnO₂ nanomaterials have been synthesized using numerous techniques. One of these is the Horizontal Vapor Phase Growth (HVPG) deposition. Recently it has been shown that the HVPG deposition is successful in synthesizing nanostructured SnO₂. However, the said technique allows the growth of many kind of structures along the length of the substrate. Thus, understanding growth mechanism of nanomaterials in HVPG technique would make it possible to control or alter the growth kinetics of the SnO₂ nanomaterial resulting to better or improved materials and devices. One idea explored is the use of external magnetic field (EMF). In this work, SnO₂ nanomaterials were synthesized using HVPG technique. The study examined the effect of EMF on the surface morphology of the synthesized nanomaterials. The surface morphology and elemental composition were investigated using Scanning Electron Microscopy (SEM) and Energy Dispersive X-ray (EDX) Analysis. Since several studies have also reported the high sensitivity of SnO₂ nanomaterials to gas reaction and adsorption, the gas sensing capabilities of the synthesized nanomaterials was explored as well. A voltage-time graph was used to measure the electrical response of the sensor substrate to CO₂ gas exposure.

2. METHODOLOGY

Five fused silica tubes with dimensions 8.6 mm inner diameter, 11.8 mm outer diameter and 292 mm length were sealed at one end using a high temperature blowtorch (a mixture of LPG and oxygen). The sealed tubes were cleaned using an ultrasonic cleanser for 30 minutes and then air-dried to remove the excess water inside the tube. Thirty five (35) milligrams of SnO₂ powder of 99% purity and <5 microns grain size obtained from Merck was loaded into the tubes. The said quartz tubes were then evacuated using a Thermionics High Vacuum System decreasing the pressure to about 10⁻⁶ Torr.

The quartz tubes were then fully sealed by annealing to a length of 15 cm.

The sealed tubes were then placed in a Thermolyne horizontal tube furnace and then annealed at 1,200°C for 8 hours. To create a temperature gradient that is necessary for the growth of the nanomaterials, the tubes were inserted halfway through the furnace. Regions of interests were designated according to their respective position in the furnace during the annealing process. The part of the tube which contained the powder and which was inside the furnace was called Section 1. The middle portion of the tube near the opening of the furnace was designated as Section 2. The last region of interest, the part of the tube that was completely out of the furnace was designated as Section 3. Each section had a length of 5 cm and was



divided into two sections, a and b as shown in fig. 1.
Fig. 1. Sealed fused quartz tube with SnO₂ powder inside sectioned into 3 sections and placed inside the furnace.

Using a type K-thermocouple, it was confirmed that section 1 was heated at 1,200°C. The temperature of section 2 was found to range from 353° to 800°C along its length, while the temperature of section 3 was found to range from 63 to 352.9°C.

Four tubes were annealed under the influence of an EMF. Sections 3a of tube 1 and 3b of tube 2 were exposed to an EMF intensity of 1900 gauss. Similarly, sections 3a of Tube 3 and 3b of tube 4 were exposed to an intensity of 3100 gauss. The EMF was supplied by a PASCO variable gap neodymium magnet with the quartz tube between two (3/4 inch diameter) cylindrical shaped permanent magnet. Tube 5, the control set-up, was annealed without the influence of EMF. The tubes were then cracked open. Nanomaterials were found to be deposited on the inner walls of the fused silica tube.

An improvised sensor setup was used for testing the CO₂ gas sensing ability of the synthesized nanomaterial. The setup consisted of a chamber with six holes for the gas inlet, gas exhaust, + and - source voltage, and electrodes of the Voltage sensor. The fused silica substrate from the setup under the

identified optimized parameter was sputtered with gold on both sides to serve as the electrodes but leaving 2mm width line in the middle of the substrate unexposed.

A Lodestar DC power supply was used to provide an input voltage of 9V with constant current of 0.5 A. A constant resistance of 10 k Ω was utilized as shown in the circuit diagram above (fig. 2).

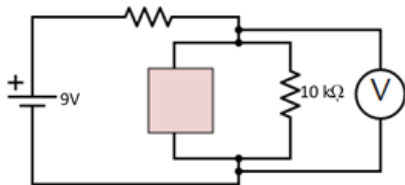


Fig. 2. Circuit diagram of the Gas Sensing Set-up

A Passport Interfaced PascoScientific Voltage Sensor and DataStudio for data acquisition was employed to measure the voltage response of the sensor. A Passport Interfaced Pasco Scientific carbon dioxide sensor was also used to monitor the amount of CO₂ gas exposed to the sensor substrate for 10s, each trial. The experimental set-up was operated at ambient temperature during the data acquisition.

3. RESULTS AND DISCUSSION

Nanoparticles were found to be dominant in the control set-up as shown in figure 3. It is observed that the nanoparticles and agglomerated nanoparticles can be found in all three sections. Aside from nanoparticles, few nanowires were seen in section 1a (Fig. 3a-3b). On the other hand, nanopole with spherical end or nanotadpole and nanowire structures were observed in section 1b in few quantity (Fig. 3c-3d). Generally, section 1 showed low density of crystal growth.

Section 2 has greater density of nanostructures compared to sections 1 and 3. Aside from nanoparticles, few wires and irregular shape structures were also deposited on section 2a (fig. 3e-3f). Meanwhile, a greater number of wires and nanotadpoles were seen in section 2b (fig. 3g-3h).

Note that section 2 has a lower temperature than section 1 by virtue of its position in the furnace. This is congruent to the results of Delos Reyes and Santos (2011), Ngo, V. T., et al (2007), and Bancolo (2011) where SnO₂ nanomaterials with different geometric structures were grown at 1200°C and a greater density of structures were seen in the middle or section 2 of the quartz tube. SnO₂ nanoparticles

are converted into agglomerated lumps and larger sized nanoparticles due to the annealing process (Sharma et al, 2009). The precipitation, nucleation and growth of nanostructures followed the Vapor-Liquid-Solid (VLS) growth where a greater number and variety of deposited structures can be found at the area near the colder regions of the furnace (Das and Jayamaran, 2014). This suggests that the temperature gradient provided the driving force for the growth of nanostructures.

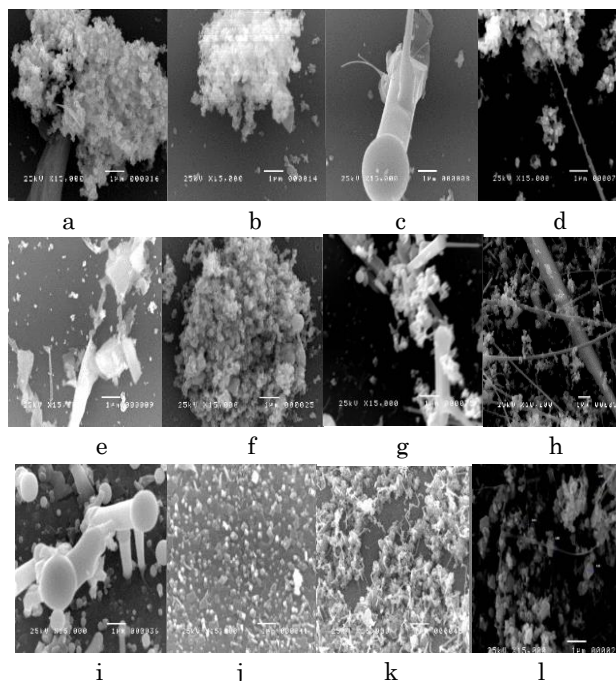


Fig. 3. Micrographs (x15,000) of nanostructures grown using HVPG without applied EMF field (a-b) section 1a, (c-d) section 1b, (e-f) section 2a, (g-h) section 2b, (i-j) section 3a, and (k-l) section 3b.

Nanotadpoles and nanowires were also seen in section 3 although in greater number than those in section 1. Section 3a showed more nanotadpoles (figure 3i-3j) while section 3b has nanowires instead (figure 3k-3l), together with agglomerated nanoparticles and spherical structure.

A different array of nanostructures can be seen in tube 4 as displayed in figure 4. Note that for this tube, only section 3b is exposed to an EMF. There were fewer nanoparticles seen in section 1 of this setup as compared to the control setup. Few nanowires and nanorods were formed in section 1a (fig. 4a-4b). Polyhedra structures and nanorods were also seen in section 1b (fig 4c-4d).

Nanoblades are dominant structures in section 2a. Nanorods, nanowires, and nanoparticles

were also formed in this section (fig. 4e-4f). Polyhedra shapes, nanorods, nanobelts, and nanowires can be observed throughout section 2b (fig. 4g-4h). Nanoparticles were also observed in the said section.

It can be noted that the EMF does not have a great effect on sections 1 and 2 because the field drops off to about 30 gauss at the outside edges of the magnet. The temperature gradient is the major driving force in the growth of nanostructures in those zones.

Few nanoparticles, with diameter ranging from 50 to 250 nanometers, were formed as well as few short nanowires, with diameter of 160 nanometers, were observed in section 3a (fig. 4i-4j).

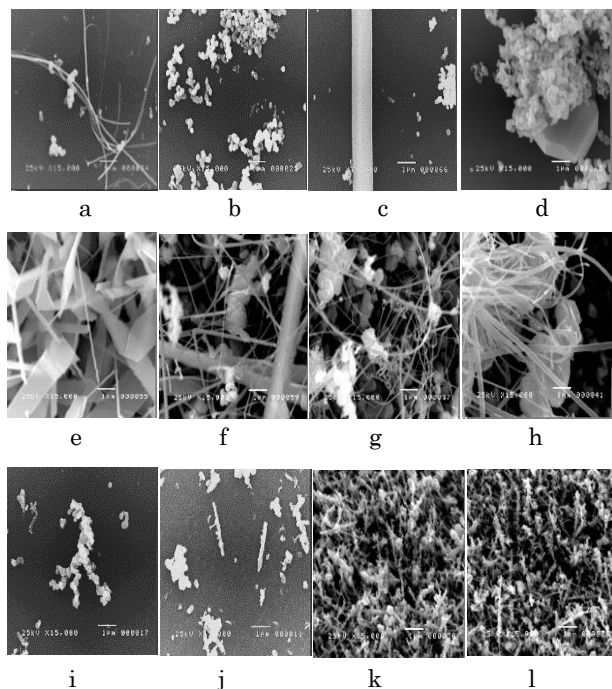


Fig. 4. Micrographs of nanostructures grown in tube 4 using HVPG (a-b) section 1a, (c-d) section 1b, (e-f) section 2a, (g-h) section 2b, (i-j) section 3a, and (k-l) section 3b.

However, when it comes to section 3b (fig. 4k-4l), where the variable gap magnet was positioned, the density of nanostructures increased with dominant nano “ferns” throughout the sample. The nanoferns are wire like structures with branches that resemble fern leaves as shown in figures 4k, 4l, and 5. Its diameter ranged from 29 to 90 nanometers and the lengths of the said structures ranged from 600 to 2000 nm. The nanoferns are observed to have greater surface-to-volume ratio, as compared to the

structures of other sections, and similar to the description of one dimensional (1D) nanostructures (Kolmakov and Moskovits, 2004).

One-dimensional oxide nanostructures (diameters below ~100 nm), like the nanoferns are expected to possess novel characteristics due to having large surface-to-volume ratio (Gubin et al, 2005). This implies that a significant fraction of the atoms (or molecules) in such systems are surface atoms that can participate in surface reactions resulting to improved selectivity and sensitivity (Kolmakov and Moskovits, 2004).

It is believed that the presence of the external magnetic field, along with the presence of temperature gradient, is responsible for the formation of the mentioned structure in section 3b. The magnetic field exposure might have retarded the nucleation rate and accelerated the crystal growth favouring nanowire formation (Bastami and Entezari, 2012). The particles interconnect with each other eventually forming the nanowire like formation (Faraji et al, 2010).

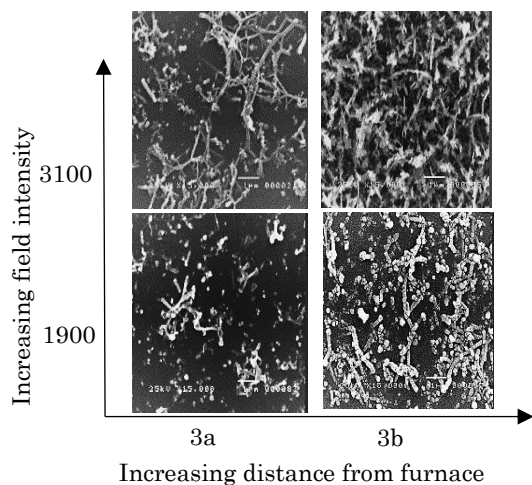
It has been reported that the nucleation and growth of magnetic materials can occur along the magnetic lines of force to form one-dimensional structures (Ji et al, 2010). Given the structure of the neodymium magnet, the magnetic lines are not parallel, which accounts for the presence of spherical structures together with the wire-like structure. The growth direction could also be led, in addition, by an epitaxial orientation defined by the substrate. Room temperature ferromagnetism has been reported in un-doped SnO₂ nanoparticles (Sharma et al, 2009; Kuznetsov et al, 2014). Diamagnetic behavior, aside from ferromagnetic behavior, has also been observed in annealed SnO₂ nanoparticles.

Most of the structures found in the zones of the previous set-up were also seen in tube 3. Tube 3 is the tube whose section 3a was exposed to an applied EMF of 3100 gauss. In section 3a of the said tube, wire like structures (38 nm to 150nm diameter) which branch out, nanoparticles, and dot like granules (46 nm to 180 nm diameter) were seen (fig. 5).

These wire like structures, mixed with some nanoparticles, were reminiscent of the nanoferns. It can be noted that the position of the magnet is near the end of the furnace where the temperature is measured to reach up to 353°C.

Similar to the previous set-up, it is believed that both the temperature gradient and the presence of external magnetic field were responsible for the formation of the wire-like structure in section 3a.

The earlier mentioned room temperature ferromagnetism in tin oxide nanoparticles has low



ferromagnetic response at high temperature (Kuznetsov et al). Reports have stated of drastic reduction in saturation magnetization when annealing temperature is increased to 400, 600, and 800°C (Kamble et al, 2013).

Fig. 5. Micrographs of structures found in sections 3a and 3b of tubes applied with 1900 and 3100 gauss EMF intensity.

In this case the annealing temperature reached is 1200°C, and the temperature of the area of the tube where the said structures were deposited is in the range of 200 to 353°C. Thus, the thermal gradient influences the material more significantly than the EMF. Meanwhile, the temperature around the permanent magnet was not able to make a permanent change to its magnetic field intensity after the annealing procedure.

With the magnet positioned at section 3a (tube 1), similar wire-like structures were seen as that of the higher applied EMF intensity counterpart (tube3). However it can be noted that the density and length of the structures (248 nm to 1.79µm) were smaller in this area (fig.5). The diameter of the said structures ranges from 40 nm to 170 nm.

Same type of structures were seen in section 3b of tube 2, exposed to an applied EMF of 1900 Gauss, as that of section 3a of tubes 1 and 3. Comparing with the yield in tube 1 whose section 3a was exposed to the same EMF intensity, there is a greater density and length (425 nm to about 3µm) of the structures in this section (fig. 10). The length of the wire, as seen in the SEM micrograph, seems to be

made of granules. The diameter of the said structure ranges from 70 nm to 265 nm.

The difference in field intensity may be responsible for the shape variation of the samples applied with EMF. However, the chain formation of the particles to form wire-like structures was seen in both setups with applied EMF of 3100 gauss and 1900 gauss. Possible reason for the variation of morphologies is the distribution of the external magnetic lines of force.

As seen in this study, higher density of nanostructure is found for the tubes with the larger fields. This is consistent with the previous report which says that the nucleation process and growth during the precipitation procedure is faster if the external magnetic field intensity is larger (Ji et al, 2010). Thus, faster crystal growth at larger field would yield higher density of structures formed.

EDX confirmed the presence of the elements of Sn and O on the crystal structures formed on the different sections of the tube in control set-up as shown in fig. 6. Different ratio of Sn and O were found in different structures.

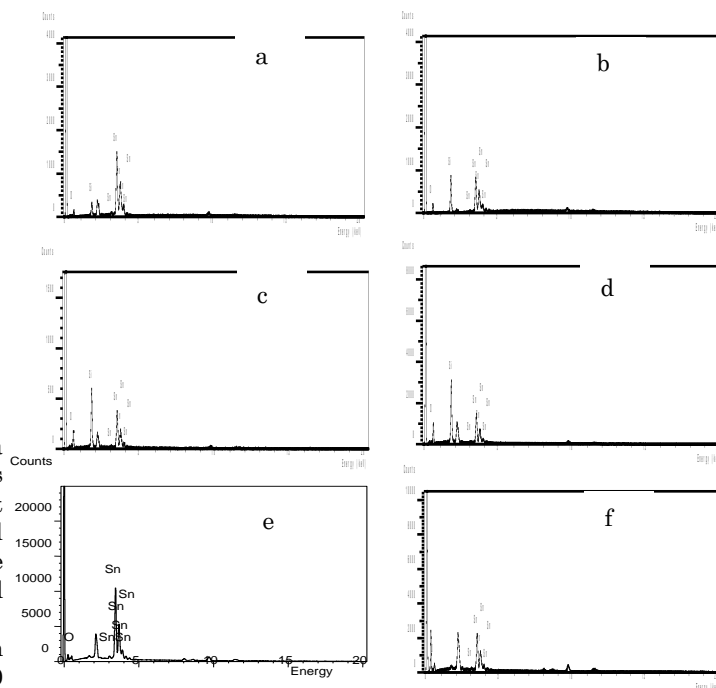


Figure 6. EDX spectrum on selected areas for sections (a) 1a (b) 1b (c) 2a (d) 2b (e) 3a (f) 3b

In 1a, the agglomerated nanoparticles has a Sn and O ratio of 4:3. While for 1b, the agglomerated nanoparticles has 1:1 ratio, suggesting that it is SnO. Similarly the nanoparticles scanned in section 2a

gave a 1:1 ratio of Sn and O. On the other hand, the same structure in section 2b gave a 1:2 ratio of Sn and O suggesting SnO₂. The nanoparticle found in section 3a was scanned to give 1:1 ratio of Sn and O. While the nanoparticles found in section 3b gave 1:3 ratio of Sn and O.

The different ratio of Sn and O suggests that the growth of the SnO₂ structure cannot be dominated by a VLS mechanism. It is suggested that the growth also occurred via a vapor-solid (VS) process which can be linked to a diffusion-limited process in a supersaturated environment (Delos Reyes, 2009; Delos Reyes and Santos, 2011; Kim and Shim, 2005).

EDX also confirmed the presence of tin oxide on the nanostructures formed on the sections of the tube applied with EMF.

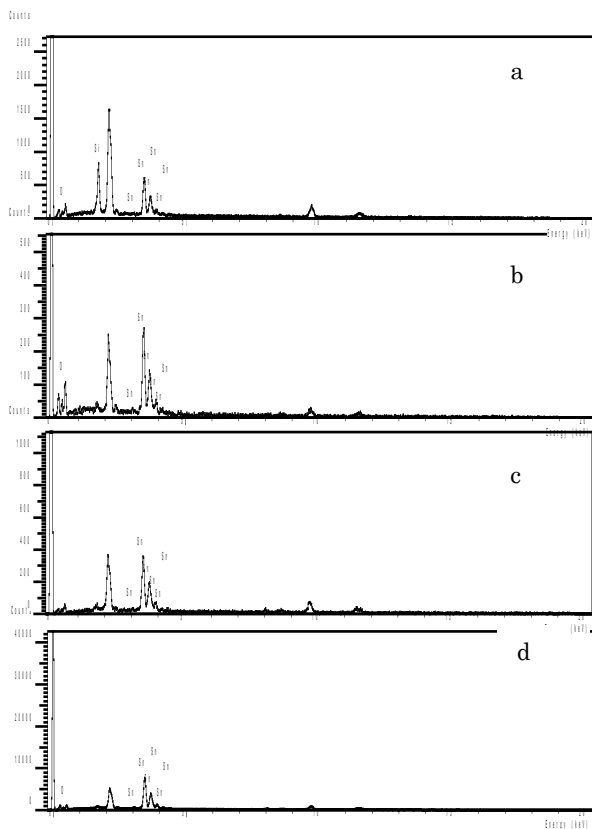


Figure 7. EDX spectrum on areas applied with 3100 gauss EMF intensity (a) on 3a (b) on 3b and 1900 gauss (c) on 3a (d) and 3b

The nanoparticles in section 3a applied with 3100 (fig. 7a) and 1900 gauss EMF intensity (fig. 7c) showed 1:2 ratio of Sn and O, indicating SnO₂. The

nanoferns found in section 3b gave a 1:1 ratio of Sn and O (fig. 7b). On the other hand, the nanoparticles scanned in section 3b applied with 1900 gauss EMF intensity (fig. 7d) was found to have 2:1 ratio of Sn and O.

The applied EMF intensity of 3100 gauss positioned at section 3b was identified to be the optimized condition due to having great surface-to-volume of the deposited structure. The gas sensing test conducted showed that the sensor can detect the presence of CO₂. As shown in figure 8, there is an increase in the voltage across the sensor whenever CO₂ is introduced. The said sensor was found to have a response time of 8-10 seconds.

Trapping of electrons at adsorbed molecules and band bending induced by these charged molecules are reported by studies to be responsible for the change in conductivity (or voltage) of the SnO₂ nanomaterials, which results to a gas response (Batzill and Diebold, 2005; Bancolo, 2011). CO₂ is an oxidizing gas which causes an increase in electrical resistance of the nanomaterial.

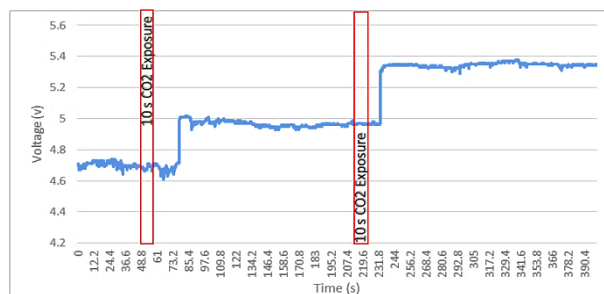


Fig. 8. Voltage measurement of the gas sensing setup as a function of time.

With constant current, any change in its resistance is proportional to a change in voltage measurement, which signals the response of the sensor. Structures with great surface to volume ratio, like the nanoferns, has greater response (change in voltage) than the control setup counterpart. High surface to volume ratio is reported to favor the adsorption of gases on the sensor and higher sensitivity due to greater interaction between the analytes and the sensing part (Cadena et al, 2007).

4. CONCLUSIONS

Application of EMF in the HVPG technique has an influence on the synthesis of SnO₂ nanomaterials. Homogenized nanoferns with high surface-to-volume ratio are produced when the EMF intensity of 3100 gauss is applied at section 3b, optimize parameter. Higher temperature section

(3a) applied with 3100 gauss intensity yielded lower density but higher diameter of wire-like structure. Lower EMF intensity produces wire-like structures with lower density. The temperature gradient has greater influence than EMF in the morphology of the nanostructure. The nanoferns sensor substrate responds to CO₂ gas.

5. ACKNOWLEDGMENTS

The authors express gratitude to Department of Science and Technology for the scholarship and support provided, as well as Ms. Prane Mariel Ong and Mr. Rey Curia.

6. REFERENCES

- A., K., & M., M. (2004). Chemical Sensing and Catalysis By One-Dimensional Metal-Oxide Nanostructures. *Annual Review of Materials Research*.
- Bancolo, F. C. (2011). Fabrication and Characterization Of Tin Oxide (SnO₂) Nanomaterials As Carbon Dioxide (CO₂) Gas Sensor. Thesis
- Bastami T. R., & Entezari M. H. (2012). Synthesis of manganese oxide nanocrystal by ultrasonic bath: Effect of external magnetic field. *Ultrasonics Sonochemistry*.
- Batzill, M., & Diebold U. (2005). The Surface and Materials Science Of Tin Oxide. *Progress in Surface Science*(79), 47–154.
- Cadena, G. J., Riu, J., & X., R. (2007). Gas Sensors Based on Nanostructured Materials. *Analyst*(132), 1083-1099.
- Das, S., & Jayaraman, V. (2014, July). SnO₂: A Comprehensive Review on Structures and Gas Sensors. *Progress in Material Science*, 66.
- De Los Reyes, R. (2009). Growth and thermal properties of Tin Oxide (SnO₂) nanomaterials prepared via horizontally vapor phase growth (HVPG) deposition. Ms Thesis.
- De Mesa, D. M., Santos, G. N., & Quiroga, R. V. (2012, August). Synthesis and Characterization of Fe₂O₃ Nanomaterials using HVPC Growth Technique for Glucose Sensing Application. *International Journal of Scientific & Engineering Research*, 3(8).
- Delos Reyes, R., & Santos, G. (2011). Growth Mechanism of SnO₂ Nanomaterials Derived from Backscattered Electron Image and EDX Observations. *International Journal of Scientific & Engineering Research*, 2(12).
- Faraji, M., Yamini, Y., & Rezaee, M. (2010). Magnetic Nanoparticles: Synthesis, Stabilization, Functionalization, Characterization, and Applications. *Journal of the Iranian Chemical Society*, 7(1), 1-37.
- Freitas, A. B., Landgraf, F. G., Seckler, M. M., & Guilietti, M. (1999). The influence of magnetic field on crystallization from solutions. *International Conference of Industrial Crystallization*. England.
- Gubin, S. P., Koksharov, Y. A., Khomutov, G. B., & Yurkov, G. Y. (2005). Magnetic nanoparticles: preparation, structure and properties. *Russian Chemical Reviews*, 74(6), 489 ± 520.
- Ji, R. P., Jiang, J. S., & Hu, M. (2010). How Does the Distribution of External Magnetic Lines of Force Influence the Growth of Ferromagnetic Material? *Journal of Physical Chemistry*.
- Kamble, V., Bhat, S., & Umarji, A. (2013). Investigating thermal stability of structural defects and its effect on d0 ferromagnetism in undoped SnO₂. *Journal of Applied Physics*, 113(24), 244 307.
- Kim, H. W., & Shim, S. H. (2005, September). Synthesis of Tin-Oxide One-Dimensional Nanomaterials and Their Characteristics. *Journal of the Korean Physical Society*, 47(3), 516~519.
- Kolmakov, A., & Moskovits, M. (2004). Chemical Sensing And Catalysis By One-Dimensional Metal-Oxide Nanostructures. *Annual Review of Materials Research*, 34, 151-180
- Kuznetsov, M. V., Belousova, O. V., Ortega, D., & Morozov, Y. G. (2014). Ferromagnetic Sn–O Nanoparticles . *Inorganic Materials*, 50(8), 793–802.
- Permanent Magnet Guidelines. (n.d.). Retrieved November 2014, from http://www.allianceorg.com/pdfs/MMPA_Magnet_Design_Guide.pdf
- Saeidi, M., Vaezzadeh, M., & Mansouri, M. (2012). Influence of AC magnetic field on phonon vibrations of superparamagnetic cluster sitting at tip end of ultra-long carbon nanotube. *Journal of Crystal Growth*.
- Sharma, A., Kumar, S., Kumar, R., Varshney, M., & Verma, K. (2009, December). Size Dependent Structural, Optical and Magnetic Properties of Un-doped SnO₂ Nanoparticles. *Optoelectronics And Advanced Materials – Rapid Communications*, 3(12).